

# Multi-Phase Reconfigurable LLC Resonant Converter with Passive Current Balancing and Wide Voltage Gain Range

Yuta Arakawa<sup>1</sup> and Masatoshi Uno<sup>1</sup>

<sup>1</sup> Ibaraki University, 4-12-1 Nakanarusawa, Hitachi, Ibaraki, Japan

**Abstract**—Voltages of lithium-ion batteries for electric vehicles vary in the range of 100–420 V depending on their state-of-charge. On-board battery chargers need a large-current capacity isolated dc-dc converter with a wide voltage gain range. Although multi-phase LLC converters are a typical solution to enhance the current capacity, additional components and feedback control loops are necessary to balance phase currents, resulting in increased circuit complexity and cost. This paper proposes the multi-phase LLC resonant converter with passive current balancing capability and wide voltage gain range. Phase currents are passively balanced thanks to the charge conservation of added flying capacitors. Furthermore, reconfigurable primary- and secondary-side circuits achieve the voltage gain range twice wider than that of conventional converters. The experimental verification using a 1-kW prototype demonstrated the passive current balancing capability as well as widened voltage gain range.

**Index Terms**—current balance, gain characteristic, multi-phase LLC converter, reconfiguration.

## I. INTRODUCTION

The demand for large-current on-board battery chargers for electric vehicles is increasing as the trend towards large-capacity lithium-ion batteries (LIBs) extends cruising distances [1]. On-board battery chargers typically comprise an ac-dc converter and an isolated dc-dc converter to connect the grid and LIBs. In general, voltages of LIBs vary in the range of 100–420 V depending on the state-of-charge, whereas the input of isolated dc-dc converters is 400 V [2]. Hence, on-board battery chargers must be an isolated dc-dc converter with a large-current capacity and wide voltage gain range of 0.25–1.05.

Multi-phase LLC converters are widely adopted as isolated dc-dc converters for large current applications thanks to their features of high efficiency, high power density, and reduced EMI. Parallel-connected multiple converters can not only enhance current capacity but also reduce input and output current ripples by operating out of phase at the same frequency. However, the gain characteristics of each converter are unavoidably mismatched to some extent due to component tolerance. Mismatched gain characteristics cause imbalanced phase currents, resulting in current concentration and increased current stress. Since the gain characteristics of LLC converters are dependent on their switching frequency  $f_s$ , pulse frequency modulation control is adopted. Parallel-connected LLC converters unavoidably operate at different  $f_s$  to maintain balanced phase currents [3].

Therefore, the interleaving technique cannot be readily applied to LLC converters.

Interleaved LLC converters with active current balancing techniques have been proposed [4]–[6]. Topologies reported in [4] and [5] can adjust resonant frequencies  $f_r$  to match gain characteristics among phases by using a variable inductor or capacitor. Multi-phase LLC converter with an additional transformer and PWM converter can unify gain characteristics by actively adjusting duty cycle  $d$  of PWM converters [6]. These topologies necessitate the integration of additional feedback control loops and current sensors, resulting in increased complexity and cost [3]–[6].

$f_s$  must vary significantly to extend the voltage gain ranges in ordinary LLC converters, bringing about a decrease in power conversion efficiency. Multi-phase LLC converters with not only extended voltage gain range by circuit reconfiguration but also passive current balancing capability have been proposed in [7]. This circuit can extend a voltage gain range by reconfiguring the primary-side circuit between a full-bridge (FB) or half-bridge (HB) inverter and the secondary-side one between a doubler (DB) or full-bridge rectifier (FBR). Reconfigurable topologies achieve a narrower range of  $f_s$  and allow the converter to operate at  $f_s$  close to  $f_r$ .

This paper proposes a multi-phase LLC resonant converter with passive current balancing capability while doubling the voltage gain range compared to [7]. Since phase currents can balance without additional current sensors nor feedback control loops by the charge conservation of flying capacitors (FCs), the proposed LLC converter achieves circuit simplification and cost reduction.

This paper is organized as follows. Section II introduces the proposed multi-phase LLC converter. Section III presents the current balancing mechanism and theoretical gain characteristic from the detailed operation analysis. The experimental verification using the 1-kW prototype will be demonstrated in Section IV.

## II. PROPOSED MULTI-PHASE LLC CONVERTER

### A. Circuit Description

Fig. 1(a) shows the proposed three-phase reconfigurable LLC converter. The transformers' primary-side circuits consist of six switching legs, three LLC resonant tanks, and two FCs ( $C_A$  and  $C_B$ ).  $C_A$  and  $C_B$  are added to the right-hand legs of Phases A and B. The

secondary-side circuits are the full-wave rectifier containing a switch  $Q_{sj}$  (where  $j$  is A, B, or C). Three phases operate at the same  $f_s$ , and Phases A and C synchronize while Phase B lags 180°.

The current capacity of the proposed multi-phase LLC converter can be arbitrarily enhanced by increasing the number of phases without redesigning, as exemplified in Fig. 1(b). Phases A and C synchronize, while Phases B and D operate 180° out of phase in the four-phase topology.

The primary-side circuit operates as either the FB or HB inverter. All switches in the FB configuration [see Fig. 2(a)] are driven with  $d = 0.5$ . In the HB configuration [see Fig. 2(b)], low-side switches ( $Q_{jL2}$ ) and high-side switches ( $Q_{jH2}$ ) in the left-hand legs are always on and off, respectively, and the right-hand legs are driven with  $d = 0.5$ . Meanwhile, the secondary-side circuit operates as either the DB or FBR.  $Q_{sj}$  is always on and off in the DB [see Fig. 3(a)] and FBR configuration [see Fig. 3(b)], respectively.

### B. Features

The proposed converter has four gain characteristics depending on the combination of the primary and secondary configurations (i.e., FB-DB, HB-DB, FB-FBR, and HB-FBR). The proposed converter achieves twice the voltage gain at the FB configuration compared with [7]. Therefore, appropriately changing the circuit configuration allows a higher voltage gain range without modifying  $f_s$  operation.

Even if gain characteristics of three phases are mismatched due to component tolerance, the charge conservation of  $C_A$  and  $C_B$  passively balances phase currents. This capability eliminates current sensors or feedback control loops and reduces system complexity and cost compared with active current balancing techniques [3]–[6].

### III. OPERATION ANALYSIS

All circuit elements are assumed ideal for simplifying the analysis, and the voltages of FCs ( $V_{CA}$  and  $V_{CB}$ ) are constant. Since the transformers' secondary-side circuit is the same as the ordinary DB and FBR configurations, this section focuses on the primary-side circuit. Operations in dead-time periods are omitted due to the page limitation.

The proposed LLC converter operates between two resonant frequencies of  $f_{r0}$  and  $f_r$ . These frequencies can be expressed as

$$f_{r0} = \frac{1}{2\pi\sqrt{(L_{kg,j} + L_{mg,j})C_{r,j}}} \quad (1)$$

$$f_r = \frac{1}{2\pi\sqrt{L_{kg,j}C_{r,j}}}, \quad (2)$$

where  $L_{kg,j}$  and  $L_{mg,j}$  are the inductances of the leakage and magnetic inductors, and  $C_{r,j}$  is the capacitance of the resonant capacitors, respectively.

#### A. Full-Bridge Configuration

The FB configuration is analyzed by focusing on FCs, resonant tanks, and switches. Figs. 4 and 5 show

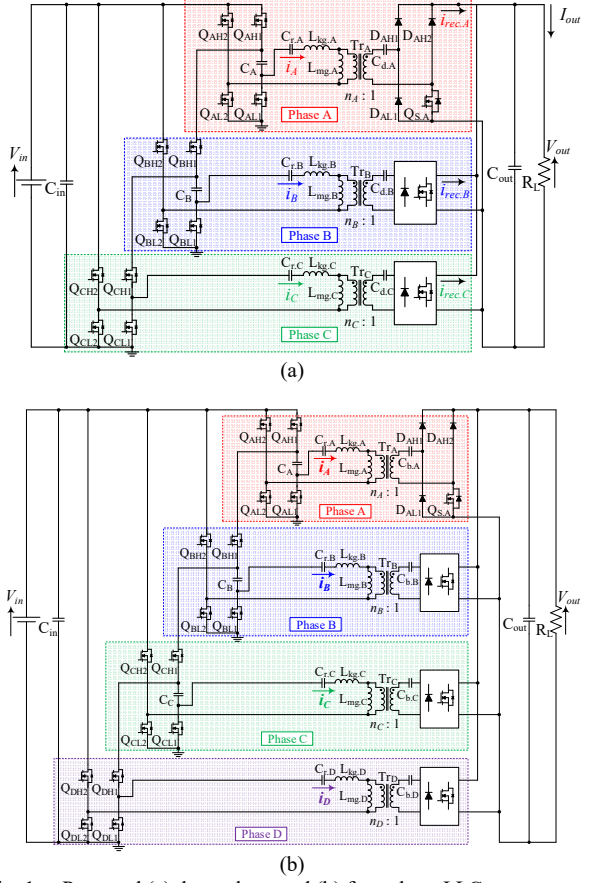


Fig. 1. Proposed (a) three-phase and (b) four-phase LLC converters.

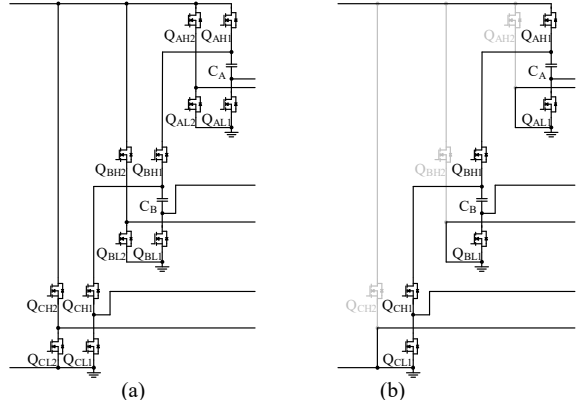


Fig. 2. Primary-side configurations as (a) FB and (b) HB.

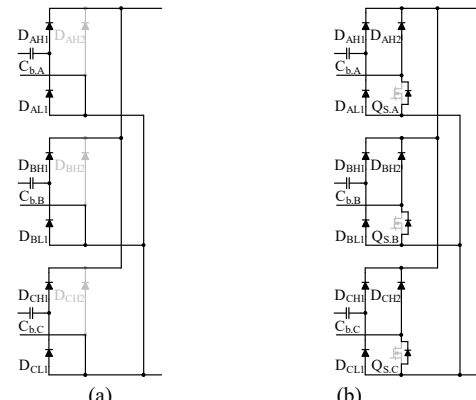


Fig. 3. Secondary-side configurations as (a) DB and (b) FBR.

theoretical key waveforms and current flow directions, respectively. The operation is roughly divided into two modes depending on switching states.

Mode 1 [Fig. 5(a)]: This mode corresponds to the positive half cycle of Phase A and C, while Phase B is in the negative half cycle.  $C_A$  and the resonant tank of Phase A are charged in series, and the resonant tank of Phase B is discharged. Simultaneously,  $C_B$  discharges toward the resonant tank of Phase C. Assuming positive and negative signs are stored and released charge, respectively, the relationship between stored and released charge amounts of the FCs and resonant tanks can be expressed as

$$\begin{aligned} q_{FC,A} &= q_A \\ -q_{FC,B} &= q_C, \end{aligned} \quad (3)$$

where  $q_{FC,j}$  and  $q_j$  are the charge amounts of the resonant tanks in Phase  $j$  and  $C_j$ , respectively. The drain-source voltages of each switch are

$$\begin{aligned} v_{QAL1} &= V_{in} - V_{CA} \\ v_{QBL1} &= V_{in} - V_{CB} \\ v_{QCL1} &= V_{CB} \end{aligned} \quad (4)$$

$$v_{QAH2} = v_{QBL2} = v_{QCH2} = V_{in}.$$

The voltage of the resonant tank,  $v_{tank.A}$ – $v_{tank.C}$ , are equal to  $v_{QAL1}$ ,  $v_{QBL2}$ , and  $v_{QCL1}$ , respectively, and therefore from (4),

$$\begin{aligned} v_{tank.A} &= V_{in} - V_{CA} \\ v_{tank.B} &= -V_{in} \\ v_{tank.C} &= V_{CB}. \end{aligned} \quad (5)$$

Mode 2 [Fig. 5(b)]: Phases A and C are in the negative half cycle, while Phase B in the positive half cycle.  $C_A$  discharges toward  $C_B$  and the resonant tank of Phase B, whereas  $V_{in}$  discharges resonant tanks of Phases A and C. The stored and released charge amounts in Mode 2 are

$$-q_{FC,A} = q_{FC,B} = q_B. \quad (6)$$

The voltage stresses of each switch are yielded as

$$\begin{aligned} v_{QAH1} &= V_{in} - V_{CA} \\ v_{QBL1} &= V_{CA} - V_{CB} \\ v_{QCH1} &= V_{CB} \\ v_{QAL2} &= v_{QBH2} = v_{QCL2} = V_{in}. \end{aligned} \quad (7)$$

$v_{tank.A}$ – $v_{tank.C}$  are equal to  $v_{QAL2}$ ,  $v_{QBL1}$ , and  $v_{QCL2}$ , respectively, and therefore from (7),

$$\begin{aligned} v_{tank.A} &= -V_{in} \\ v_{tank.B} &= V_{CA} - V_{CB} \\ v_{tank.C} &= -V_{in}. \end{aligned} \quad (8)$$

According to charge conservation of  $C_A$  and  $C_B$ , combining  $q_{FC,A} = -q_{FC,A}$ ,  $q_{FC,B} = -q_{FC,B}$ , (3) and (6) yields

$$q_A = -q_B = q_C. \quad (9)$$

$-q_B$  means Phase B is  $180^\circ$  out of phase. Since (9) means the charge amounts in three phases are matched, all phase currents can be passively balanced.

Average voltages of the resonant tank of Phases  $j$  are ideally zero under steady-state conditions. Combining (5) and (8) produces

$$\begin{aligned} V_{CA} &= \frac{2}{3}V_{in} \\ V_{CB} &= \frac{1}{3}V_{in}. \end{aligned} \quad (10)$$

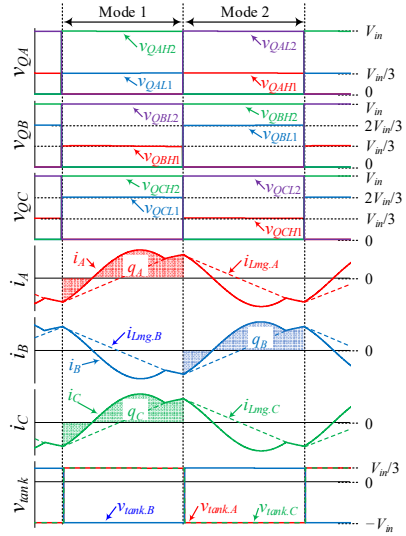


Fig. 4. Theoretical key waveforms in FB configuration.

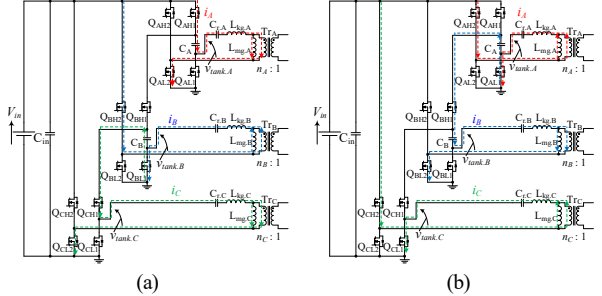


Fig. 5. Current flow directions in FB configuration in (a) Mode 1 and (b) Mode 2.

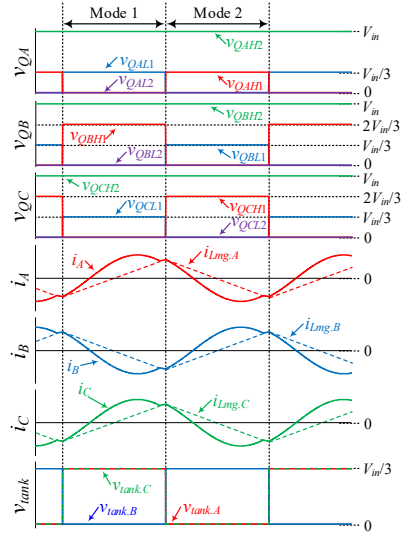


Fig. 6. Theoretical key waveforms in HB configuration.

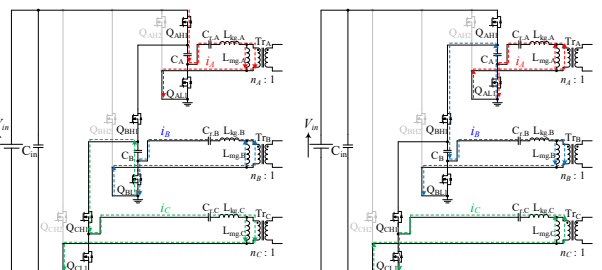


Fig. 7. Current flow directions in HB configuration in (a) Mode 1 and (b) Mode 2.

## B. Half-Bridge Configuration

Figs. 6 and 7 show theoretical key waveforms and current flow directions in the HB configuration. The operation is divided into two modes similar to that in the FB configuration.

Mode 1 [Fig. 7(a)]: The high-side switches ( $Q_{AHI}$  and  $Q_{CHI}$ ) and the low-side switch ( $Q_{BLI}$ ) are on.  $V_{in}$  charges  $C_A$  and the resonant tank of Phase A in series. On the other hand,  $C_B$  discharges towards the resonant tank of Phase C. The relationship of the stored and released charge amounts of  $C_A$ ,  $C_B$ , and the resonant tanks of each phase can be expressed as (3). The switches' voltage stress is given by (4) and (7). Since  $v_{tank,j}$  are always equal to  $v_{QjL1}$ ,

$$\begin{aligned} v_{tank.A} &= V_{in} - V_{CA} \\ v_{tank.B} &= 0 \\ v_{tank.C} &= V_{CB}. \end{aligned} \quad (11)$$

Mode 2 [Fig. 7(b)]: The low-side switches ( $Q_{AL1}$  and  $Q_{CL1}$ ) and the high-side switch ( $Q_{BHI}$ ) are on.  $C_B$  and the resonant tank of Phase B are charged by  $C_A$ . The relationship of the stored and released charge amounts can be expressed as (6). The combination of (3) and (6) yields (9). Therefore, the proposed converter in the HB configuration can passively balance all phase currents. Since the switches' voltage stress in Mode 2 is equal to (4) and (7),  $v_{tank,j}$  is expressed as

$$\begin{aligned} v_{tank.A} &= 0 \\ v_{tank.B} &= V_{CA} - V_{CB} \\ v_{tank.C} &= 0. \end{aligned} \quad (12)$$

## C. Gain Characteristics

The proposed converter can be considered simply connected in parallel by assuming all the resonant tanks are identical. Hence, the proposed converter can be converted into the single-phase equivalent circuit, as shown in Fig. 8(a).  $C_{r,tot}$ ,  $C_{b,tot}$ ,  $L_{kg,tot}$ , and  $L_{mg,tot}$  are combined parallel capacitance or inductance.

$$\begin{aligned} C_{r,tot} &= 3C_r, \quad C_{b,tot} = 3C_b, \\ L_{kg,tot} &= \frac{L_{kg}}{3}, \quad L_{mg,tot} = \frac{L_{mg}}{3}, \end{aligned} \quad (13)$$

where  $C_b$  is the capacitance of the dc blocking capacitors on the secondary-side circuit.  $f_{r0}$  and  $f_r$  of the equivalent circuit are given by combining (1), (2), and (13) as

$$f_{r0} = \frac{1}{2\pi\sqrt{(L_{kg,tot} + L_{mg,tot})C_{r,tot}}} \quad (14)$$

$$f_r = \frac{1}{2\pi\sqrt{L_{kg,tot}C_{r,tot}}} \quad (15)$$

Four gain characteristics in the proposed converter can be derived by analyzing the equivalent circuit of Fig. 8(a) based on fundamental harmonic approximation [8].

The peak-to-peak value of  $v_{tank,j}$  in the FB configuration is  $4V_{in}/3$  as can be seen by (5) and (8), whereas the HB configuration's one is  $V_{in}/3$  from (11) and (12) [see Fig. 8(a)]. Thus, amplitudes of the fundamental harmonic component of  $v_{tank}$ ,  $V_{m,tank}$ , are given by Fourier series as

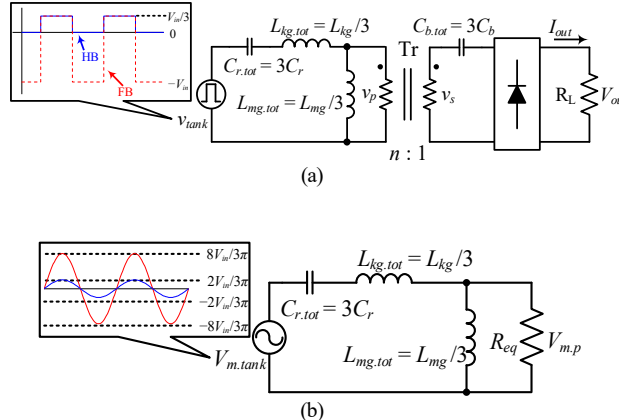


Fig. 8. (a) Equivalent circuit of proposed LLC converter and (b) Fourier-transformed one.

$$\begin{aligned} V_{m,tank(FB)} &= \frac{2}{\pi} \frac{4V_{in}}{3} \\ V_{m,tank(HB)} &= \frac{2}{\pi} \frac{V_{in}}{3}. \end{aligned} \quad (16)$$

The secondary winding voltage  $v_s$  in the DB and FBR configurations are square wave voltages with the peak-to-peak value of  $V_{out}/2$  and  $V_{out}$ , respectively. Converting to the peak-to-peak value of the primary winding voltage  $v_p$  ( $= nv_s$ ) yields  $nV_{out}/2$  and  $nV_{out}$ , respectively. Therefore, amplitudes of the fundamental harmonic component of  $v_p$ ,  $V_{m,p}$ , are

$$\begin{aligned} V_{m,p(DB)} &= \frac{2n}{\pi} \frac{V_{out}}{4n} \\ V_{m,p(FBR)} &= \frac{2}{\pi} V_{out}, \end{aligned} \quad (17)$$

where  $n$  is the turns ratio.  $R_{eq}$  is identical to those of ordinary LLC converters and defined as

$$\begin{aligned} R_{eq(DB)} &= \frac{2n^2}{\pi^2} R_L \\ R_{eq(FBR)} &= \frac{8n^2}{\pi^2} R_L, \end{aligned} \quad (18)$$

where  $R_L$  is the load resistance.

The proposed LLC converter can be expressed as the Fourier transformed equivalent circuit with  $V_{m,tank}$  and  $R_{eq}$  shown in Fig. 8(b). From the equivalent circuit, four voltage gains  $G$  ( $= nV_{out}/V_{in}$ ) are

$$G_{FB-DB} = \frac{nV_{out}}{V_{in}} = \frac{4}{3} \frac{V_{m,p(DB)}}{V_{m,tank(FB)}} = \frac{4}{3} X, \quad (19)$$

$$G_{FB-FBR} = \frac{2}{3} X, G_{HB-DB} = \frac{1}{3} X, G_{HB-FBR} = \frac{1}{6} X$$

$$X = \frac{4}{3} \frac{1}{\sqrt{\left[1+A\left(1-\frac{f_r^2}{f_s^2}\right)\right]^2 + \left[Q_L\left(\frac{f_s}{f_r}-\frac{f_r}{f_s}\right)\right]^2}}, \quad (20)$$

where  $A$  and  $Q_L$  are defined by

$$A = \frac{L_{kg,tot}}{L_{mg,tot}} \quad (21)$$

$$Q_L = \frac{1}{2\pi R_{eq} f_r C_{r,tot}}. \quad (22)$$

Fig. 9 shows theoretical gain characteristics of four configurations under the same load condition. Gain

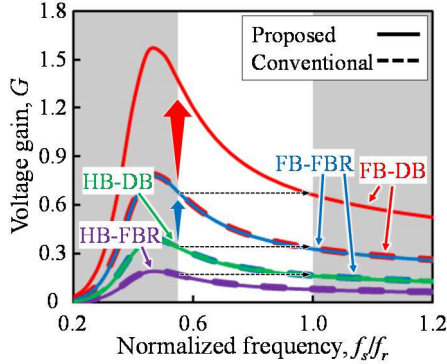


Fig. 9. Comparison of voltage gain ranges.

characteristics of the HB-DB, FB-FBR, and FB-DB are two, four, and eight times higher than that of the HB-FBR configuration. Gain characteristics in the FB configuration are twice that reported in [7] because  $V_{m,tank(FB)}$  in (16) is double compared with the conventional one.

#### IV. EXPERIMENTAL RESULTS

A 1-kW prototype of the proposed converter was designed and built, as shown in Fig. 10. Table I lists its component values. Key parameters of  $L_{kg,j}$ ,  $L_{mg,j}$ , and  $n$  of three transformers were intentionally severely mismatched to verify the passive current balancing capability.

Fig. 11 shows the measured current waveforms of  $i_A - i_C$  in the FB-DB (500 W) and HB-DB configurations (200 W) at  $V_{in} = 200$  V and  $f_s = 130$  kHz. Despite the severe mismatch in the transformer parameters, the current error among the three phases was less than 4% and 2% in the FB-DB and HB-DB configurations, respectively.

Fig. 12 shows the measured gain characteristics of four configurations, where  $f_{r,ave}$  is the average resonant frequency of each phase. These configurations were operated in the range of  $f_s = 80$ – $170$  kHz. The voltage gain in each configuration was about two, four, and eight times higher than the HB-FBR. In addition, the voltage gain range of 0.25–1.05 ( $V_{out} = 100$ – $420$  V) was covered by reconfiguring primary- and secondary-side circuits.

#### V. CONCLUSION

This paper has proposed the multi-phase LLC resonant converter with passive current balancing capability and wide voltage gain range. Phase currents can balance thanks to the charge conservation of the flying capacitors. Furthermore, reconfiguring the primary- and secondary-side circuits allows for widening the voltage gain range. In addition, doubling the voltage gain range compared to the conventional converter.

The experimental verification using a 1-kW prototype demonstrated not only the passive current balancing capability even with the severe mismatch in the transformers' parameters but also the reconfigurable circuits widened the voltage gain range.

Our future works include detailed operation analyses about the three-phase interleaved topology by applying the asymmetric resonant operation to reduce further the input and output current ripple [9].

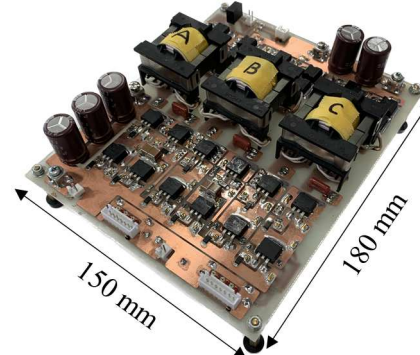


Fig. 10. Photograph of 1-kW prototype.

Table I  
COMPONENT VALUES

Components	Value
Switches	MOSFET, $R_{on} = 70$ mΩ
$C_A$ and $C_B$	Ceramic capacitor, $2.2\ \mu F \times 4$
$C_{b,A}$ – $C_{b,C}$	Ceramic capacitor, $2.2\ \mu F$
$C_{r,A}$ – $C_{r,C}$	Film capacitor, $100\ nF$
$C_{in}$	Aluminum electrolytic capacitor, $47\ \mu F \times 3$
$C_{out}$	Aluminum electrolytic capacitor, $47\ \mu F \times 3$
Diodes	Schottky diode, $V_F = 1.05$ V
$T_{rA}$	$n_A = 1.97$ , $L_{kg,A} = 8.42\ \mu H$ , $L_{mg,A} = 49.6\ \mu H$
$T_{rB}$	$n_B = 2.03$ , $L_{kg,B} = 10.02\ \mu H$ , $L_{mg,B} = 58.9\ \mu H$
$T_{rC}$	$n_C = 1.86$ , $L_{kg,C} = 7.83\ \mu H$ , $L_{mg,C} = 43.5\ \mu H$
$f_{r,A}$ – $f_{r,C}$	$f_{r,A} = 173$ kHz, $f_{r,B} = 159$ kHz, $f_{r,C} = 180$ kHz

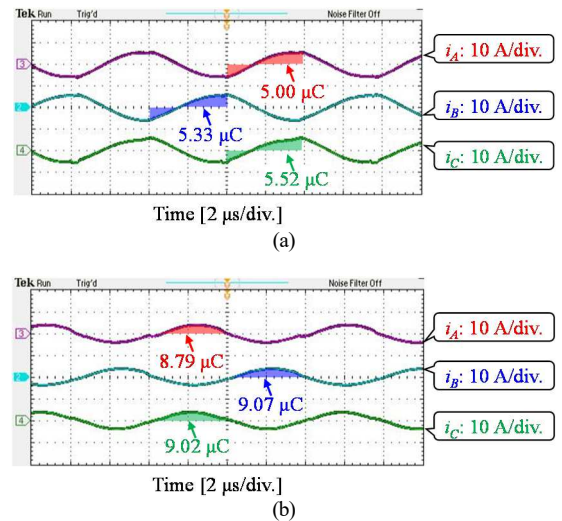


Fig. 11. Measured current waveforms in (a) FB-DB and (b) HB-DB configurations.

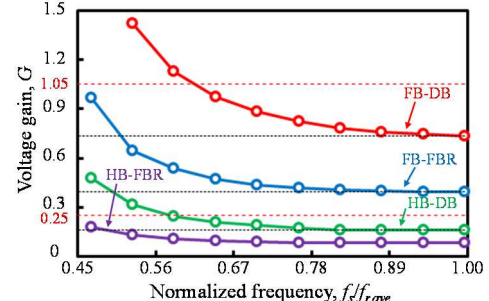


Fig. 12. Measured gain characteristics of four configurations.

#### ACKNOWLEDGMENT

This research was granted by the Institute of Electrical Engineers of Japan for the IEEJ Sakurai Fund for International Exchange Travel.

#### REFERENCES

- [1] M. Yilmaz, and P. T. Krein, "Review of battery charger topologies, charging power levels, and infrastructure for plug-in electric and hybrid vehicles," *IEEE Trans. Power Electron.*, vol. 28, no. 5, pp. 2151–2169, May 2013.
- [2] G. Liu, Y. Jang, M. Jovanovic, J. Q. Zhang, "Implementation of a 3.3-kW DC–DC converter for EV on-board charger employing the series-resonant converter with reduced-frequency-range control," *IEEE Trans. Power Electron.*, vol. 32, no. 6, pp. 4168–4184, Jun. 2017.
- [3] G. Yang, P. Dubus, and D. Sadarnac, "Double-phase high-efficiency, wide load range high-voltage/low-voltage LLC dc/dc converter for electric/hybrid vehicles," *IEEE Trans. Power Electron.*, vol. 30, no. 4, pp. 1876–1886, Apr. 2015.
- [4] E. Orietti, P. Mattavelli, G. Spiazzi, C. Adragna, and G. Gattavari, "Two-phase interleaved LLC resonant converter with current-controlled inductor," in Proc. *Brazilian Power Electron. Conf.*, pp. 298–304, Sep. 2009.
- [5] Z. Hu, Y. Qiu, L. Wang, and Y. Liu, "An interleaved LLC resonant converter operating at constant switching frequency," *IEEE Trans. Power Electron.*, vol. 29, no. 6, pp. 2931–2943, Jun. 2014.
- [6] H. Chen, X. Wu, and S. Shao, "A current-sharing method for interleaved high-frequency LLC converter with partial energy processing," *IEEE Trans. Ind. Electron.*, vol. 67, no. 2, pp. 1498–1507, Feb. 2020.
- [7] K. Koyama and M. Uno, "Automatic current balancing multi-phase reconfigurable LLC converter with wide voltage gain range for on-board battery charger," in Proc. *IEEE Energy Conversion Congress and Exposition (ECCE)*, pp. 2176–2183, Oct. 2021.
- [8] T. Duerbaum, "Design-oriented steady-state analysis of LLC resonant converters based on FHA," in Proc. *IEEE Int. SPEEDAM*, pp. 200–207, May 2006.
- [9] Y. Tada, M. Uno, and Y. Sato, "Three-phase interleaved LLC asymmetric resonant converter with capacitive current balancing and reduced switch voltage stress," *IEEE Access.*, vol. 8, pp. 5688–5698, Dec. 2019